Recurring types of variability and transitions in the ~620 kyr record of climate change from the Chew Bahir basin, southern Ethiopia

Martin H. Trauth*[1], Asfawossen Asrat[2], Andrew S. Cohen[3], Walter Duesing[1], Verena Foerster[4], Helen Roberts[5], Stefanie Kaboth-Bahr[1], Hauke Kraemer[1,6], Henry F. Lamb[5], Norbert Marwan[6], Mark A. Maslin[7], Frank Schaebitz[4]

[1] University of Potsdam, Institute of Geosciences, Potsdam, Germany

[2] Addis Ababa University, School of Earth Sciences, Addis Ababa, Ethiopia

[3] University of Arizona, Department of Geosciences, Tucson, USA

[4] University of Cologne, Institute of Geography Education, Cologne, Germany

[5] Aberystwyth University, Department of Geography and Earth Sciences, Aberystwyth, UK

[6] Potsdam Institute for Climate Impact Research, Potsdam, Germany

[7] University College London, Geography Department, London, UK

*Corresponding Author: email trauth@uni-potsdam.de, Tel. +49 331 977 5810, Fax +49 331 977 5700

Abstract

The Chew Bahir Drilling Project (CBDP) aims to test possible linkages between climate and hominin evolution in Africa through the analysis of sediment cores that have recorded environmental changes in the Chew Bahir basin (CHB). In this statistical project we used recurrence plots (RPs) together with a recurrence quantification analysis (RQA) to distinguish two types of variability and transitions in the Chew Bahir aridity record and compare them with the ODP 967 wetness index from the eastern Mediterranean. The first type of variability is one of slow variations with cycles of ~20 kyr, reminiscent of the Earth's precession cycle, and subharmonics of this orbital cycle. In addition to these cyclical wet-dry fluctuations in the area, extreme events often occur, i.e. short wet or dry episodes, lasting for several centuries or even millennia, and rapid transitions between

these wet and dry episodes. The second type of variability is characterized by relatively low variation on orbital time scales, but significant century-millennium-scale variations with progressively increasing frequencies. Within this type of variability there are extremely fast transitions between dry and wet within a few decades or years, in contrast to those within Type 1 with transitions over several hundreds of years. Type 1 variability probably reflects the influence of precessional forcing in the lower latitudes at times with maximum values of the long (400 kyr) eccentricity cycle of the Earth's orbit around the sun, with the tendency towards extreme events. Type 2 variability seems to be linked with minimum values of this cycle. There is no systematic correlation between Type 1 or Type 2 variability with atmospheric CO_2 concentration. The different types of variability and the transitions between those types had important effects on the availability of water, and could have transformed eastern Africa's environment considerably, which would have had important implications for the shaping of the habitat of *H. sapiens* and the direct ancestors of this species.

Introduction

Some hypotheses about the relationship of climate and human evolution suggest that episodes of increased climate variability (e.g. Potts, 1996, 2013, Maslin and Trauth, 2009) or prominent transitions (e.g. Vrba, 1985, 1993) may have enhanced rates of speciation, dispersal and technological innovation. Examples on long time scales are the termination of the permanent El Nino/establishment of the modern Walker/Hadley circulation between 3.5–2.0 Ma, possibly linked to the closure of the Indonesian sea way (Cane and Molnar, 2001; Ravelo et al., 2004; Trauth et al., 2009), and the intensification of the Northern Hemisphere Glaciation at 2.75 Ma (e.g., Bonnefille, 2010; Trauth et al., 2009), both being subject to lively discussions during the last four decades (Vrba 1985, 1983; deMenocal 1995, 2004; Brovkin and Claussen, 2008; Kröpelin et al., 2008a,b; Trauth et al., 2005, 2009). As the most recent example of a major climate shift in the tropics, in particular in Africa, the termination of the African Humid Period (AHP, ~15–5 kyr BP) has also been intensely investigated, in particular the extent to which it was abrupt or gradual (deMenocal et al., 2000; Kuper and Kröpelin, 2006; Tierney and deMenocal, 2013; Trauth et al., 2018), which is important for potential migration scenarios within and across the Sahara and cultural transformations (Kuper and Kröpelin, 2006).

52 Revived by these debates, statistical methods have recently been used to make quantitative statements about

53 the degree of variability and character of transitions. According to their analysis, the most important transition

54 during the long-term trend towards a more arid climate was at ~1.9 Ma, at about the time of the establishment

55 of the modern Walker/Hadley circulation (Ravelo et al., 2004; Trauth et al., 2009), and not, as suggested earlier

56 by deMenocal (1995, 2004) during the intensification of the Northern Hemisphere Glaciation (INHG). Similarly,

57 the termination of the AHP at ~5 kyr BP was tested for its relative abruptness comparing observed and

58 theoretical probability distributions of paleoclimate time series from multiple locations in and around Africa

59 (Tierney and deMenocal, 2013). According to their analysis, the wet-dry transition occurred within centuries,

60 which agrees with the results of Trauth et al. (2018) using a change point analysis to determine a ~880 yr

61 interval within which this important climate shift occurred.

62

63 More sophisticated approaches to classifying variability and transitions were used by Trauth et al. (2019) with

64 recurrence plots together with a recurrence quantification analysis on six short (<17 m) sediment cores

65 collected during the Chew Bahir Drilling Project (CBDP) from the Chew Bahir basin (CHB) in southern Ethiopia,

66 reaching back to ~47 kyr BP. Recurrence plots (RPs) are graphic displays of recurring states in the

67 environmental system (Eckmann et al. 1987; Marwan et al. 2007). Quantitative descriptions (measures of

68 complexity) have been developed to complement visual inspection of recurrence plots (RPs) and for

69 recurrence quantification analysis (RQA) (e.g. Zbilut and Webber 1992; Marwan et al. 2007; Marwan 2008).

70 Trauth et al. (2019) presented and discussed results from such an RQA on the environmental record of the

71 CHB short cores. The different types of variability and transitions in these records were classified to shed light

72 on our understanding of the response of the biosphere to climate change, particularly the response of humans

73 in the area.

74

75 One of the most interesting transitions examined with the RP/RQA was once again the termination of the

76 African Humid period (Trauth et al., 2018, 2019). The rapid (~880 yr) change of climate in response to a

77 relatively modest change in forcing appears to be typical of tipping points in complex systems such as the

78 Chew Bahir basin (Lenton et al., 2008; Ditlevsen and Johnsen, 2010). If this is the case then 14 dry events at

79 the end of the AHP, each of them 20–80 yrs long and recurring every 160±40 yrs as documented in the Chew

80 Bahir cores could represent precursors of an imminent tipping point which, if properly interpreted, would allow

81 predictions to be made of future climate change in the Chew Bahir basin (Trauth et al., 2018, 2019). Compared

82 to the low-frequency cyclicity of climate variability before and after the termination of the AHP, this type of

83 cyclicity occurs on time scales equivalent to a few human generations. In other words, it is very likely (albeit

84 speculative) that people were conscious of these changes and adapted their lifestyles to the consequent

85 changes in water and food availability. A deeper analysis of our data is however required to understand

86 whether the wet-dry climate transition in the area was due to a saddle-node bifurcation in the structural stability

87 of the climate, or whether it was induced by a stochastic fluctuation (Lenton et al., 2008; Ditlevsen and

88 Johnsen, 2010).

89

90 Here we present a RP/RQA-based analysis of two long (~290 m) cores collected in 2014 in the Chew Bahir

91 basin (4°45'40.55"N 36°46'0.85"E), spanning the time from ~620 kyr to present. The Chew Bahir basin is

92 situated in a transition zone between the Main Ethiopian Rift and the Omo-Turkana basin, adjacent to the

93 Lower Omo Basin, where some of the oldest known fossils of anatomically modern humans were found

94 (McDougall et al., 2005). According to recent archeological findings, the adjoining highlands in the area may

95 have been a refuge area for groups of *H. sapiens* during times of climatic stress (Ambrose et al., 1998; Brandt

96 and Hildebrand, 2005; Vogelsang et al., 2018; Ossendorf et al., 2019).

97

98 We compare the Chew Bahir record of environmental change during the past ~620 kyr with the wetness index

99 for the wider northeastern Saharan/North Africa from ODP Site 967 (Grant et al., 2017). The site was drilled

100 during ODP Leg 160 in the eastern Mediterranean (34°N, 34°E, 2,252 m water depth), where Saharan and

101 North African dust and Nile riverine input are the primary contributors of sediment. The ODP 967 wetness

102 index is a combined run-off and dust signal in a single metric, reflecting the effects of both

103 strengthening/northward migration (increased run-off) and weakening/southward retreat (increased dust) of

104 the northern and northeastern African monsoon (Grant et al., 2017). The catchment of the Nile River with its

105 two tributaries, the White Nile and the Blue Nile, extends from southeastern Africa to parts of the northwestern

106   Ethiopian highlands. In the very wet phases, the Lakes Abaya-Chamo-Chew Bahir-Turkana system with its

107   connecting rivers drained into the Nile catchment (Junginger et al., 2013). Therefore, both the upper Nile

108   catchment and the Chew Bahir catchments are in spatial proximity and are most likely exposed to similar

109   climate fluctuations and their causes. Humid conditions, recorded in both ODP 967 and CHB cores, could

110   indicate the regional significance of a wet phase. Similar patterns in the types of variability and transitions

111   could be indicative of the effect of a similar climate dynamic.

112

113   As a contribution to the reconstruction of environmental conditions for eastern Africa based on long terrestrial

114   sediment records, our CHB record is firstly used to classify variability down core in order to identify recurring

115   episodes of stable wet or dry, of cyclic or more complex but predictable variability, and of chaotic/random

116   variability. Second, we classified types of transitions, including episodes with no change, linear/gradual shifts

117   with different rates of change, as well as different types of rapid transitions such as tipping points. As soon as

118   a classification of variability and transitions is available, one can discuss possible reasons for the similarity,

119   e.g. similar boundary conditions such as global ice volume, local insolation, atmospheric CO_2 levels and ocean

120   sea-surface temperatures. Finally, we hypothesize which types of variability and transitions may have affected

121   the biosphere including hominins.

Materials and methods

The Middle Pleistocene–Holocene paleoclimate record of the Chew Bahir basin

124   The sediment cores described herein were collected in the western part of the Chew Bahir basin in the

125   southern Ethiopian Rift (4.1–6.3°N, 36.5–38.1°E, ~500 above sea level; Fig. 1). Chew Bahir is a tectonic basin,

126   separated from the Lower Omo basin to the west by the Hammar Range, which is the source of most of the

127   sediments at the coring site. This range to the west and the highlands to the north and north-east consist of

128   Late Proterozoic granitic and mafic gneisses, whereas the eastern part of the catchment is dominated by

129   Miocene basaltic lava flows. Oligocene basalt flows with subordinate rhyolites, trachytes, tuffs and ignimbrites

130   cover the Precambrian basement units in the distal north-eastern, northern, and north-western parts of the

catchment (Moore and Davidson, 1978; Davidson, 1983). Being a closed basin, Chew Bahir forms a terminal sink for weathering products from its 32,400 km^2 catchment.
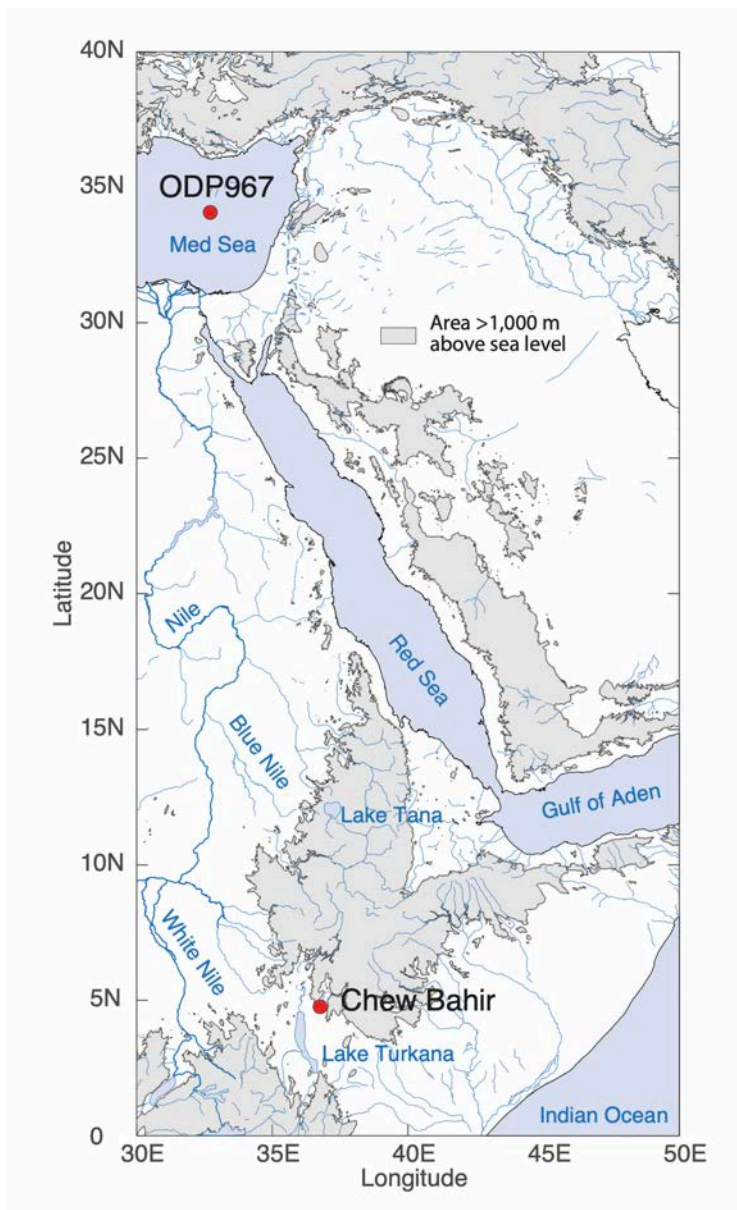
Figure 1 Map of northeastern Africa and adjacent areas showing the location of the Chew Bahir basin (4°45'40.55"N 36°46'0.85"E, ~500 m above sea level), the ODP Leg 160 Site 967 in the eastern Mediterranean Sea (34°4'6"N 32°43'31"E, ~2,254 m water depth), and the river Nile with its two tributaries the White and Blue Niles connecting both regions. Coastline and river polygons from the Global Self-consistent, Hierarchical, High-resolution Geography data set (GSHHG) (Wessel and Smith 1996). Topography from the 1 arc-minute global relief model of the Earth's surface (ETOPO1) (Amante and Eakins 2009).

142   The present-day climate in eastern and northeastern Africa is influenced by a number of major air streams and

143   convergence zones, with their effects superimposed on regional influences associated with topography, large

144   lakes, and the oceans (Nicholson, 2017). Rainfall in the Chew Bahir catchment is associated with the passage

145   of the tropical rain belt, resulting in a strongly bimodal annual cycle. Most of the moisture reaching the Ethiopian

146   highlands in June–August comes from the Mediterranean and Red Sea (55%), and from the Indian Ocean

147   (31%) (Viste and Sorteberg, 2013). Short-term (annual to decadal) fluctuations in the intensity of precipitation

148   relate to E-W adjustments in the zonal Walker circulation associated with the El Niño-Southern Oscillation

149   (ENSO) and the Indian Ocean Dipole (IOD), possibly as a direct response to sea-surface temperature (SST)

150   variations in the Indian and Atlantic Oceans, which are in turn affected by the ENSO and the IOD (Nicholson,

151   2017).

152

153   The paleoclimate of Chew Bahir was first reconstructed using six short cores, up to ~17 m long and collectively

154   spanning ~47 kyr, which were collected in 2009–2010 (Foerster et al., 2012, 2015; Trauth et al., 2015, 2018,

155   2019). In the context of the Hominin Sites and Paleolakes Drilling Project (HSPDP) to drill at key fossil hominin

156   and archeological sites (Cohen et al., 2016; Campisano et al., 2017), we collected parallel, duplicate cores:

157   HSPDP-CHB14 2A (4°45'40.32"N 36°46'0.48"E) and 2B (4°45'40.68"N 36°46'1.20"E) in the Chew Bahir basin,

158   266.38 and 278.58 m long, respectively, in Nov–Dec 2014 (Foerster et al., in prep; Schäbitz et al., in prep). A

159   292.87 m long composite core of the Chew Bahir Drilling Project (CBDP) with more than 90% recovery was

160   created from the duplicate cores.

161

162   The composite core was developed by merging the two parallel cores 2A and 2B by core-to-core correlation

163   using MSCL logs, core images, lithological description and XRF data sets. Radiometric age constraints were

164   based on ^{14}C dating of ostracodes, optically stimulated luminescence (OSL) dating of fine-silt sized quartz

165   grains, and single-crystal total-fusion (SCTF) ^{40}Ar/^{39}Ar dating of feldspars from tuffaceous zones within the

166   core. In addition, a volcanic ash layer identified in the core has been correlated on the basis of major and minor

167   element geochemistry to a dated tephra found in the outcrop at Konso, in the southern Main Ethiopian Rift,

168   namely the Silver Tuff (Roberts et al., in prep.). The ages generated are stratigraphically consistent, and

169   Bayesian age-depth modeling incorporating ^{14}C, OSL and [40]Ar/[39]Ar ages, and tephrochronological data has

170   been used to build an age model for the Chew Bahir cores (age model *RRMay2019*, Roberts et al., in prep.).

171

172   We analyzed the potassium (K) concentrations of the sediment, determined by micro X-ray fluorescence

173   (µXRF) scanning which was previously shown to be a reliable proxy for aridity in the Chew Bahir basin

174   (Foerster et al., 2012; Trauth et al., 2015, 2018). The most likely process linking climate with K concentrations

175   is the authigenic illitization of smectites during episodes of higher alkalinity and salinity in the closed-basin lake

176   resulting from a drier climate (Foerster et al., 2018). After processing the µXRF data to remove coring and

177   scanning artifacts, the data were corrected for outliers and jumps, before we applied various types of

178   normalizations and standardizations of the data (Foerster et al., in prep.).

179

180   *Principles of recurrence plots (RP) and recurrence quantification analysis (RQA)*

181   As a first approximation we can describe the Chew Bahir paleolake as a complex system composed of

182   interacting components, such as the water body, the sediment below the bottom of the lake, and the organisms

183   living in the lake and its surroundings (Marwan et al., 2007; Trauth et al., 2019). This multi-dimensional system

184   is characterized by many state variables such as precipitation (with more rain causing higher weathering and

185   erosion of rocks in the catchment, and hence more potassium (K) washed into the lake), evaporation (causing

186   higher K concentrations in the sediment through authigenic K fixation in smectites, Foerster et al., 2018) and

187   wind speed (blowing higher quantities of K-rich particles from the catchment into the lake).

188

189   One way to unfold the dynamics of the multi-dimensional system from one-dimensional time series is time-

190   delay embedding, whereby the dynamic characteristics of the system are preserved (Packard et al., 1980).

191   The reason for a complete reconstruction of the system from a single variable is that the information about the

192   system and its state variables is contained in the one-dimensional time series. The embedding of the time

193   series in a three-dimensional (m=3) phase space, for example, means that three successive values with a

194   temporal distance τ (or *tau*) are represented as a point in a three-dimensional coordinate system (the phase

195   space) (Iwanski and Bradley, 1998; Webber and Zbilut, 2005; Marwan et al., 2007). The phase space portrait

then displays the embedded time series of observations as a trajectory in the phase space, i.e. the phase space trajectory represents the path over which the system's state evolves through time. The reconstruction of the phase space (from embedding) is not exactly the same as the original phase space (the true variables describing the lake), but its topological properties are preserved, provided that the embedding dimension is sufficiently large (Packard et al., 1980; Takens, 1981).

A common feature of dynamical systems is the property of recurrence (Webber and Zbilut, 2005). Patterns of recurring states of a system reflect typical system characteristics whose description contributes significantly to understanding the system's dynamics. A recurrence plot (RP), introduced by Eckmann et al. (1987), is a graphical display of such recurring states of the system, calculated from the distance (e.g. Euclidean) between all pairs of observations, within a cutoff limit (Marwan et al., 2007). To complement the visual inspection of recurrence plots, measures of complexity were introduced for their quantitative description to perform the recurrence quantification analysis (RQA) (e.g., Marwan et al., 2007; Marwan, 2008). Among these, a selection of measures based on the recurrence density, others based on diagonal and vertical lines typically appearing in recurrence plots are very useful for studying the behavior of the Chew Bahir lake system. As an example of measurements based on the recurrence density, the *recurrence rate* (*RR*) is the density of black dots in the recurrence plot. This measure simply describes the probability of recurring states of the system in a particular time period.

Diagonal lines in recurrence plots typically occur when a segment of the trajectory runs almost (e.g. within a given tolerance) in parallel to another segment, representing an earlier episode of the system's history in the phase space, for a certain period of time. Diagonal lines in recurrence plots are therefore diagnostic of cyclic behavior in time series, and in contrast to the time series analysis using Fourier-based methods, this cyclic behavior is not restricted to sinusoidal structures when using recurrence plots. Since cyclic behavior can be used to predict future conditions from the present and past, the ratio of the recurrence points that form diagonal structures (of a minimum length) to all recurrence points is therefore a measure for *determinism* (*DET*, or predictability) of the system. Vertical lines in recurrence plots typically correspond to periods where the

223   trajectory remains in the same phase space region (Marwan et al., 2007; Marwan 2010). Vertical lines are

224   therefore diagnostic of episodes when the state of the system does not change or changes very slowly. In

225   other words, the system seems to be trapped in a specific state for some time, which is typical for irregular

226   transitions between different types of dynamics.

Results

228   Recurrence plots (RPs), together with a recurrence quantification analysis (RQA), were used to describe

229   different types of environmental variability and transitions in the Chew Bahir (Fig. 2 and Suppl. Fig. 1–6). From

230   the available RQA measures we have selected RR and DET because they describe important properties of

231   the dynamic Chew Bahir system but are very descriptive compared to other RQA measures (Marwan et al.,

232   2007; Trauth et al., 2019). We compare the RPs and RQA measures of the Chew Bahir record with those of

233   the wetness index for the wider northeastern Saharan/North African record from ODP 967 (Grant et al., 2017)

234   (Fig. 3).

235

236   We have used K as a proxy for aridity, as the dominant process linking climate with K concentrations is the

237   authigenic illitization of smectites during episodes of higher alkalinity and salinity in the closed-basin lake

238   resulting from a drier climate (Foerster et al., 2018). For the analysis of the ~620 kyr record the K record was

239   embedded in a phase space with a dimension of m=6 and temporal distances of τ=5, equivalent to 5×0.1

240   kyr=0.5 kyr, where 0.1 kyr is the resolution of the time series following a piecewise cubic Hermite interpolating

241   polynomial (Frisch and Carlson, 1980). We use the window size w=500 and the step size ws=50 data points

242   of the moving window to calculate the RQA measures (Fig. 2). The size w of the window corresponds to

243   500x0.1 kyr=50 kyr and the step size is 50x0.1 kyr=5 kyr. To compare the RP/RQA based dynamics in the

244   Chew Bahir record of aridity with the wetness index of ODP 967, we interpolated the marine record to the

245   same time axis, used an embedding dimension of m=2 and temporal distances of τ=2 to create the RPs and

246   the same window size to calculate the RQA measures (Fig. 3). We use a slightly lower embedding dimension

247   m and τ because the signal-to-noise ratio of the ODP 967 moisture index seems to be lower than that of the

248   K record of Chew Bahir, as experiments with different values for m and τ showed. Similarities in the texture of
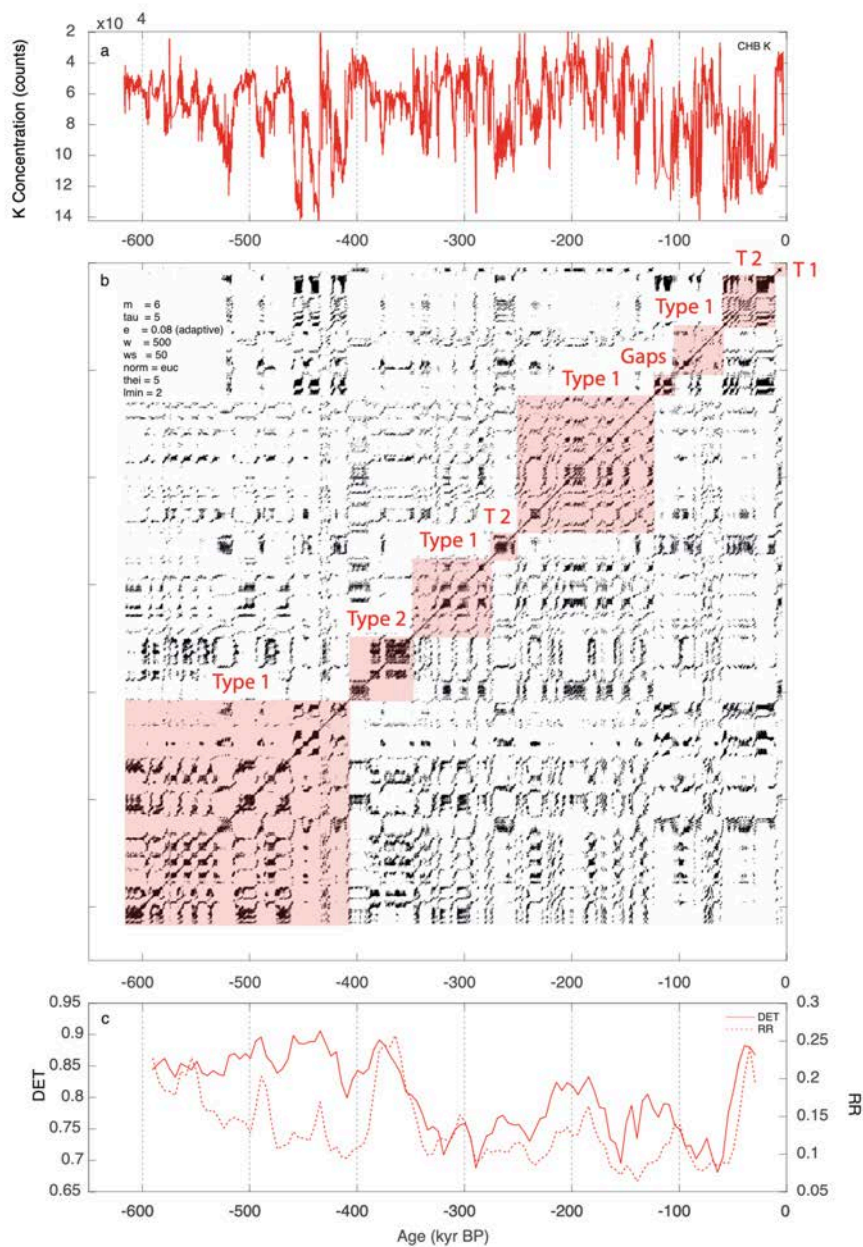
249

Figure 2 Recurrence plot (RP) and recurrence quantification analysis (RQA) measures of the potassium (K) concentrations of the sediment in Chew Bahir, southern Ethiopia: the time series according to age model (3) (upper panel), the recurrence plot (middle panel) and the RQA measures of moving windows (lower panel). Embedding parameters *m*=embedding dimension, *tau*=time delay, *e*=threshold, *w*=window size, *ws*=window moving steps, *norm*=vector norm, *thei*=size of Theiler window, *lmin*=minimum line length, RQA measures *RR*=recurrence rate and *DET*=determinism. See the methods section for a detailed description of the embedding parameters and RQA measures.
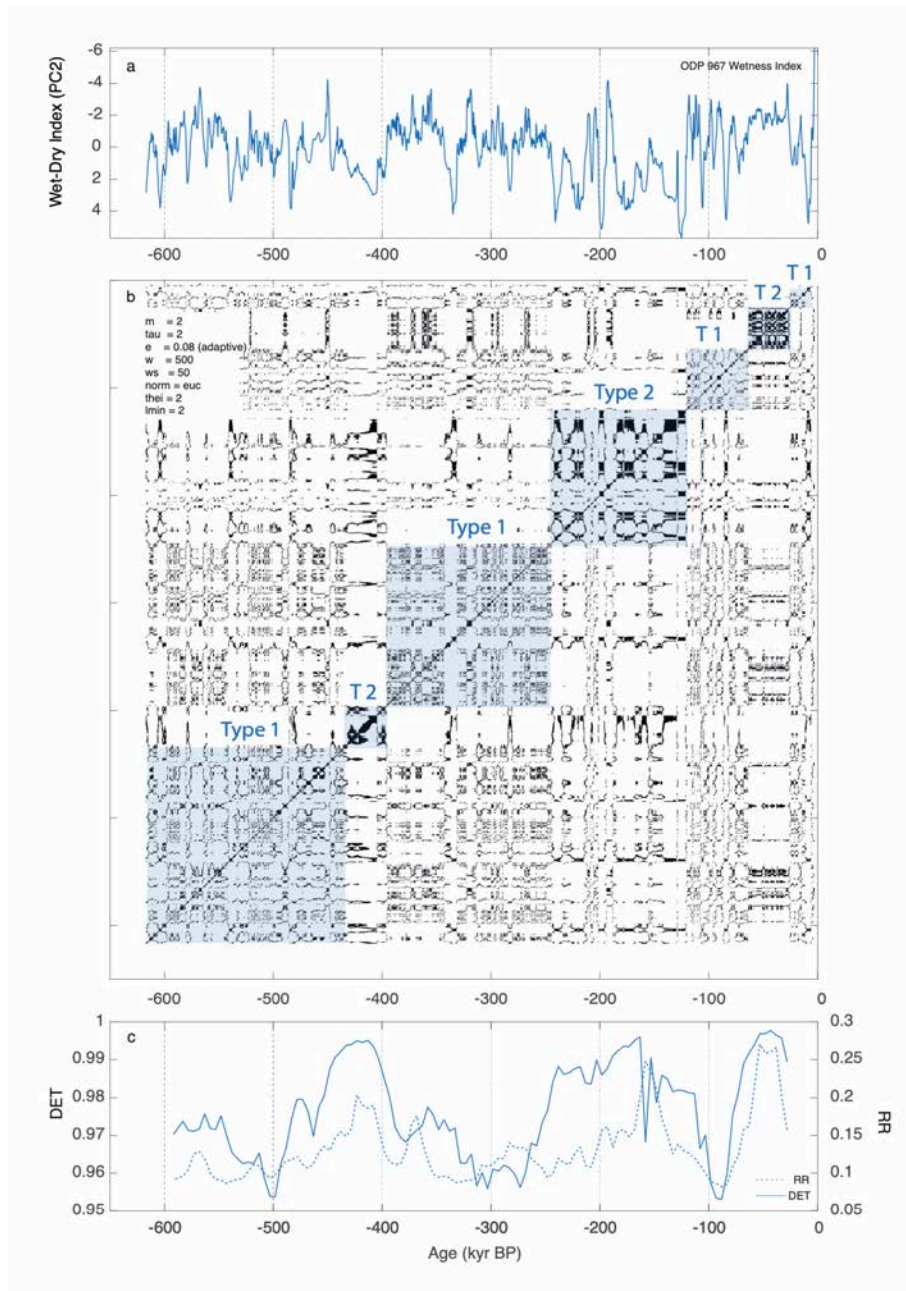
Figure 3 Recurrence plot (RP) and recurrence quantification analysis (RQA) measures of the ODP 967 wetness index according to Grant et al. (2017) from the eastern Mediterranean: the time series (upper panel), the recurrence plot (middle panel) and the RQA measures of moving windows (lower panel). See previous figure for the meaning of the abbreviations. For abbreviations, see caption of Figure 2. See the methods section for a detailed description of the embedding parameters and RQA measures.

the recurrence plots of both proxy records show that the embedding provides comparable results with these values. However, even identical embedding parameters would not lead to significantly different results.

The first series of four clusters of recurrence points occurs between 620 and 410 kyr BP in the Chew Bahir record, with the largest cluster between 620 and 462 kyr BP, then three smaller clusters at 456–435, 435–425, and 425–410 kyr BP (Fig. 2). These clusters are characterized by a series of *s*-shaped diagonal lines, overlain by blocks with high recurrence rates, which mark 1–2 kyr long episodes of relative stability. The diagonal lines are interrupted by white vertical lines, reflecting a series of wet-dry episodes recurring with approximately half-precession cyclicity, initiated and terminated by relatively abrupt transitions. As the result of the cyclic recurrence of wet and dry conditions, the DET values are relatively high (~0.85), whereas RR has moderate, but declining values (0.2–0.1). Two extremely dry episodes centered at ~455 and ~438 kyr BP are reflected in two clusters of recurrence points and high DET values (~0.9) within the 458–436 kyr BP interval, separated by white vertical lines and slightly lower DET values. Zooming into the interval between 620 and 410 kyr BP with higher (0.025 kyr) resolution the diagonal lines become blurred and the RP is dominated by many small (<10 kyr) blocks that are connected by black horizontal and vertical lines (Suppl. Fig. 1). This suggests that, at time scales of <10 kyr, the system oscillates between shorter stable states, each 1–5 kyr long, with rapid transitions between them. Within the blocks, we observe diagonal lines indicating high-frequency (<1 kyr) cyclicities. In the ODP 967 wetness index we find a similar type of variability in the time before 435 kyr, although in comparison diagonal structures are much less pronounced or even absent (Fig. 3). The RR values are at similar values to those in the Chew Bahir, except for a significant anticorrelation at ~420 kyr (Fig. 4). The DET values are generally lower but increase after ~500 kyr BP up to similar values as in the Chew Bahir record.

This interval ends with a rapid transition at ~410 kyr BP from dry to wet conditions. This transition is followed by two dense clusters of recurrence points between 410 and 348 kyr BP, indicating episodes of a stable wet climate with extreme RR and DET values, interrupted by short dry episode at ~375 kyr BP (Fig. 2). The two clusters reflect relatively stable humid conditions, with the humidity level in the first cluster being higher than in the second cluster and hence the two clusters are separated by a transition towards a slightly less wet

Page 13

climate at around 390 kyr BP. The second cluster is interrupted by a distinctive dry event at around 376 kyr

BP. Interestingly, both clusters show an irregular pattern of diagonal lines, partly slightly curved, suggesting

recurrent dry events, but with slightly variable cyclicity. Zooming into the interval between 410 and 348 kyr BP

with higher (0.025 kyr) resolution we observe blurred diagonal lines with 1–2 kyr distances, indicating a weak

cyclicity on millennium time scales even within the otherwise quite stable wet episodes (Suppl. Fig. 2). The

interval between 410 and 348 kyr BP is terminated by gradual (~10 kyr) transition towards slightly more humid

conditions after ~348 kyr BP. The ODP 967 wetness index indicates similar wet conditions during this episode,

but with almost no form of variability (Fig. 3). As a consequence, the RR values are relatively high (~0.2)

whereas the DET values are also at high level but relatively low compared to before and after the event (~0.97).

The next cluster of recurrence points between 348 and 272 kyr BP is marked by a series of blocks with weak

internal structure and separated by white vertical lines (Fig. 2). This structure reflects a series of relatively

stable wet conditions, interrupted by several thousand-year long dry episodes, some of which are bounded by

relatively rapid transitions from wet to dry and back. The occasional appearance of diagonal lines, though

rarely parallel to the main diagonal, indicates weak cyclic behavior. Within this interval the RR values are

constantly low (~0.1–0.15), whereas the DET values start at high values (~0.97) and decline until about 320

kyr BP before they remain at low values (~0.7). Zooming into the interval between 348 and 272 kyr BP with

higher (0.025 kyr) resolution confirms the observation of small blocks connected with black horizontal and

vertical lines in the RP, as a result of a rapid change between relatively stable dry and wet conditions, with the

exception of the block between 330 and 327 kyr BP. This block is merely the result of a gap that was closed

by interpolation (Suppl. Fig. 3). The blocks themselves have little internal structure, with the exception of very

weak diagonal lines with a spacing of <1 kyr. The interval between 348 and 272 kyr BP is terminated by a very

rapid transition from wet to dry conditions at ~272 kyr. The ODP 967 wetness index shows a similar variability

type during this episode, with DET values declining parallel to those of the Chew Bahir (Fig. 3).

Between 272 and 252 kyr BP, we observe another dense cluster of recurrence points (Fig. 2). The internal

structure of this block is reminiscent of similar structures of the clusters at ~400 and ~360 kyr BP, whereas the

system state based on the difference in the DET values does not support this conclusion. The interval again shows diagonal lines, this time very clearly curved, with slight convergence with respect to the main diagonal. As a result of the distinct cyclicity, the RR and DET values are at moderate levels, with DET at a local maximum. This pattern suggests that the climate was relatively stable, but fluctuations between humid and dry occur in cycles. These changes occur more and more frequently over time, until the climate finally quickly changes to generally humid conditions at around 228 kyr BP. Zooming into the interval between 272 and 252 kyr BP with higher (0.025 kyr) resolution reveals that the curved diagonal lines are rather a sequence of short, laterally offset diagonal pieces. In the younger section of the block, the diagonal lines disappear (Suppl. Fig. 4). Considering the course of the time series it can be seen that the diagonals reflect increasingly shorter wet phases, and until after about 236 kyr quite stable, relatively dry conditions prevail in the Chew Bahir. The ODP 967 wetness index shows similar climate fluctuations during this episode, but these are too unclear to be described with a different type of variability (Fig. 3). The RR values are low, similar to those in the Chew Bahir, whereas the DET values are possibly at a local maximum, again similar to Chew Bahir.

The RPs of the following episode between 252 and 122 kyr BP show a blocky pattern with complex internal structure and many white vertical lines (Fig. 2). Again, we observe short diagonal lines, causing slightly higher DET values. This episode mirrors the earlier ones between 620 and 410 kyr BP and between 348 and 272 kyr BP, whereby in the second interval also the state of the environmental system also recurs. The episode is unfortunately followed by two gaps due to core loss between ~122 and 107 kyr BP, which are filled by the interpolation with curves, so we get a high RR at this point that we cannot interpret (Fig. 2). Zooming into the interval between 252 and 122 kyr BP with higher (0.025 kyr) resolution reveals many small blocks surrounded by *s*-shaped curved structures rather than continuous diagonal lines which mark short (<5 kyr) wet phases which begin and end gradually (Suppl. Fig. 5). Besides that, we observe longer (5–10 kyr) wet episodes with rapid onset and termination, internally structured by converging diagonals, structurally similar to the ones in the interval between 272 and 252 kyr BP, but with a different system state based on the RR and DET values. This interval is terminated by ~5 kyr long gaps after 122 kyr BP. During this episode, the ODP 967 wetness index shows a type of variability that is more similar to the episode of 435 and 370 kyr BP, rather than the one
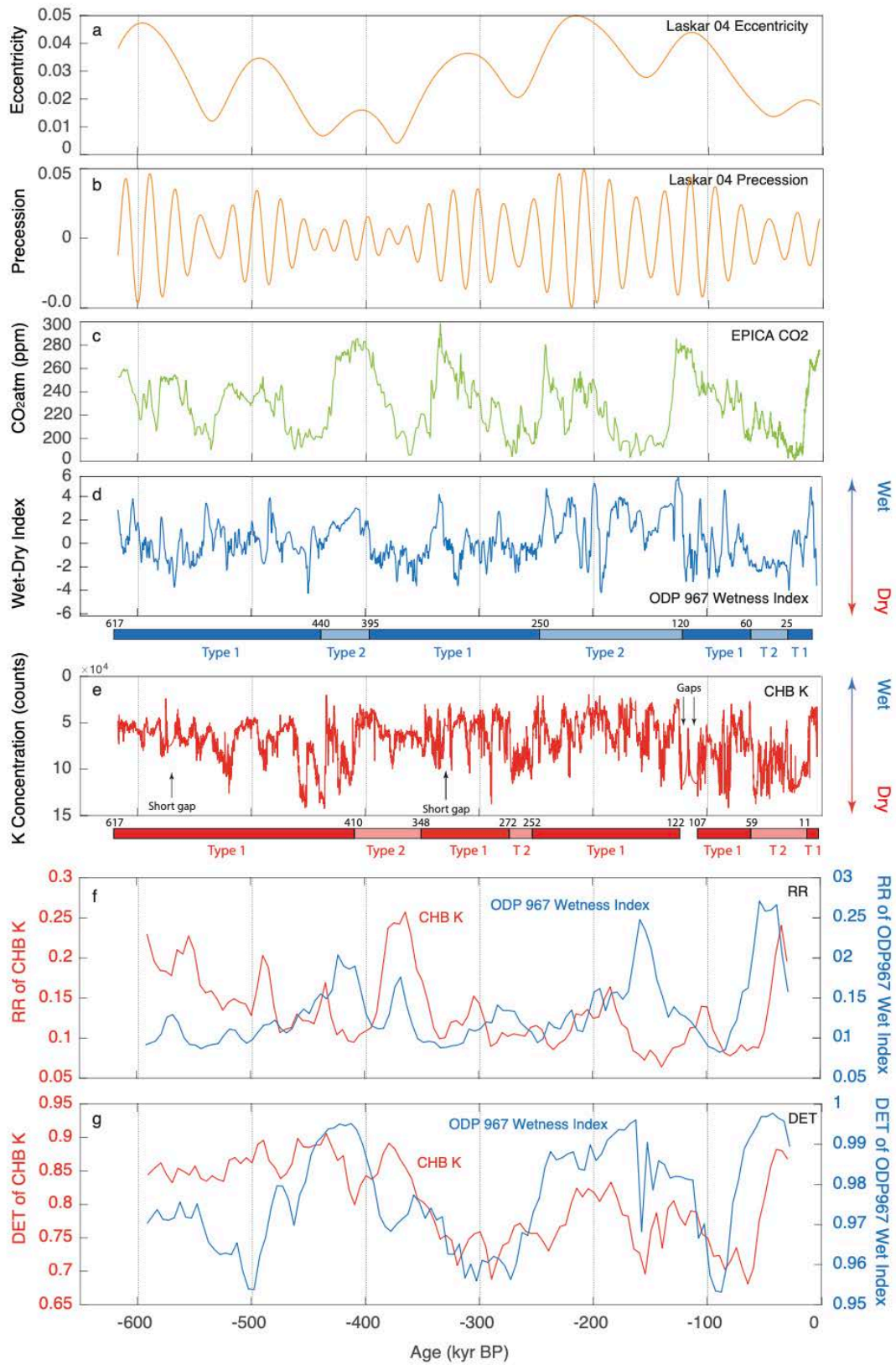
Figure 4 Comparison of the complex dynamics of variations in aridity in southern Ethiopia with strengthening/northward migration and weakening/southward retreat of the North African monsoon. **(a+b)** Earth's eccentricity and precession cycle (Laskar et al., 2004); **(c)** Antarctica EPICA Dome C atmospheric CO_2 according to Bereiter et al. (2015); **(d)** ODP 967 wetness index according to Grant et al. (2017); **(e)** Chew Bahir aridity derived from the potassium (K) concentrations of the sediment in Chew Bahir using age model *RRMHT500* (Roberts et al., submitted), note the reverse y-axis; **(f+g)** comparison of RQA measures determinism (DET) and recurrence rate (RR) of the recurrence plots (RP) of the Chew Bahir aridity record (in red) and ODP 967 wetness index (in blue). DET is a measure of the predictability of the system and RR describes the probability of recurring states of the system in a particular time period.

after 370 kyr BP (Fig. 3). The course of the RR values is similar to the one of Chew Bahir in the first half of the interval, but seems to be anticorrelated in the second half. The DET values show a very similar pattern to those of the Chew Bahir, although at lower levels (~0.98–0.99 at ODP 967, ~0.75–0.8 at Chew Bahir). The increasing DET values at the beginning of the interval are about 20 kyr later for ODP 967, then they vary in a very similar way even including a minimum at about 160 kyr, and then decline at the end of this interval (Fig. 4).

Between 107 and 59 kyr BP, we find a very complex phase with fast changes between stable humid, very variable humid and very dry conditions, each separated by fast transitions (Fig. 2 and Suppl. Fig. 6). After a very dramatic transition we observe very regular climate fluctuations between ~59 kyr BP and about 11 kyr BP, when it became relatively stable dry. This interval is again characterized by a cluster of dense recurrence points, slightly converging diagonal lines which indicate increasing recurrence rates (i.e. shorter wet-dry cycles), before we see a black block of recurrence points as the result of very stable dry conditions. The last ~11 kyr are characterized by very wet conditions, interrupted with a short, about ~1 kyr long dry intervals and terminated by a transition towards a dry climate. The distinct cyclic alternation of wet and dry conditions, each of which are ~5 kyr long, results in high RR and DET values. The last ~47 kyr BP are preserved at higher resolution in the short cores from the same basin, also examined with the method of RP/RQA (Trauth et al., 2019). Here we found very similar patterns as on the long time scale, with alternating appearances of blocky structures and diagonal lines, with different transitions between episodes. The ODP 967 wetness index here shows a similar variability with long-periodic, high amplitude fluctuations between wet and dry between ~120 and 60 kyr BP, followed by an episode without such variations (Fig. 3). The time interval between 60 and 25

376 kyr BP is relatively stable, as compared with the high-frequency variability observed in the Chew Bahir, before

377 we observe two long wet cycles, out of which the second one is also seen in the Chew Bahir record.

Discussion

379 We applied a detailed analysis of the RPs together with a RQA to distinguish between different types of climate

380 variability, and transitions in the Chew Bahir basin (Trauth et al. 2018) (Fig. 4). Here, climate is inferred from

381 our key proxy, the potassium concentration of the sediment representing the relative aridity in the Chew Bahir

382 Basin (Foerster et al., 2018). Our statistical analyses herein are a contribution to an accurate picture of

383 environmental change in eastern Africa during the last ~620 kyr and thereby provide a quantitative, high

384 resolution climatic component useful for investigating human-climate interactions. The fossil and

385 archaeological record of eastern Africa is still too limited to draw definitive conclusions with respect to current

386 hypotheses on the relationship between climate and evolutionary patterns in humans and other animals.

387 However, our results do allow for some initial comparisons and hypotheses (e.g. Stringer and Galway-Witham,

388 2017; Scerri et al., 2018; Galyway-Witham et al., 2019).

389

390 Our analysis clearly shows a number of different types of variability in the K record that overlay a long-term

391 trend towards greater aridity and variability (Figs. 2 and 4). These types of variability are separated by

392 transitions, which are of varying types of durations and structures. Many of these types, both variability and

393 transitions, occur multiple times during the last ~620 kyr, so it is interesting to investigate them more closely

394 to see if they are characteristic of the Chew Bahir Basin or possibly occur even beyond the region. In addition,

395 it is important to examine whether these types are linked to certain regional or global boundary conditions (e.g.

396 global ice volume, atmospheric CO_2 levels, ocean sea-surface temperatures) (Fig. 4).

397

398 We observe two basic types of variability that do not mix, but each form a series of variants. The first type of

399 variability, occurring at 620–410 kyr BP, 348–272 kyr BP, 252–122 kyr BP, and (after a period with no data)

400 107–59 kyr BP, are slow variations with cycles of ~20 kyr and subharmonics of this cycle, as indicated by the

401 occurrence of diagonal lines with 20 kyr, 10 kyr, and 5 kyr spacing (Figs. 2 and 3). In addition to these cyclical

402   wet-dry fluctuations in the area, extreme events often occur, i.e. short wet or dry episodes, lasting for several

403   centuries or even millennia, and rapid transitions between wet and dry episodes. This type of variability

404   probably reflects the influence of precessional forcing in the lower latitudes at times of increased eccentricity,

405   with a tendency towards extreme events. This also shows in comparatively low RR and DET values,

406   suggesting a lower predictability of climate variations for this type of variability. This type of variability correlates

407   with maximum values of the long (400 kyr) eccentricity cycle, and hence maximum variability in the precession

408   frequency band. There is no systematic correlation with atmospheric CO_2 concentration.

409

410   The second type of variability, occurring at 410–348 kyr BP, 272–252 kyr BP, and 59–11 kyr BP, is

411   characterized by relatively low variation on orbital time scales. Instead, we observe significant century-

412   millennium-scale variations with increasing frequency in the course of an episode with Type 2 variability, as

413   the curved diagonal lines in RP suggest (Figs. 2 and 3). The very prominent cycles in the frequency band lead

414   to very high DET and partly high RR values, which indicate a high predictability of climate change, much higher

415   than at times of Type 1. Within this type of variability there are extremely fast transitions between dry and wet

416   within a few decades or years, in contrast to those within Type 1 with transitions that last several hundreds of

417   years. Type 2 variability seems to be linked with minimum values of the long (400 kyr) eccentricity cycle, and

418   again there does not seem to be a link with atmospheric CO_2 levels. The first episode with Type 2 variability

419   occurs in an interval with maximum eccentricity in the 100 kyr frequency band when the atmospheric CO_2 was

420   quite high. The other two episodes occur during minimal eccentricity in this frequency band, with low CO_2

421   levels at the same time.

422

423   The ODP 967 wetness index shows a very similar type of variability, with RR values that highly resemble the

424   variations in the Chew Bahir record, except for the prominent anticorrelation at ~420 and ~150 kyr BP (Fig. 4).

425   The DET values fluctuating in a smaller range (0.95–1.00) compared to those of the Chew Bahir (0.65–0.95),

426   but the temporal variations of DET show obvious similarities at both sites, in particular during the last ~350

427   kyr. Since the age models of both sites have large uncertainties, it is not possible at this point to judge

428   conclusively whether time shifts in the DET curves are the result of poor age control or actual differences in

climate dynamics recorded in the two locations. Comparing the temporal occurrence of the different types of variability in both localities, the ODP 967 wetness index shows a Type 2 variability approximately during the first and third episode of Type 2 variability in the Chew Bahir record, but not during the second episode of Type 2 variability in the Chew Bahir. Instead we find a Type 2 variability between ~245 and 120 kyr BP in the ODP 967 wetness index, all with high DET and RR values. The different types of variability, very obvious in the RPs, but differing slightly in the RQA measures, could also indicate actual differences in dynamics, but also the influence of the spline interpolation on the temporal autocorrelation.

Overall, the K curve shows a clear trend towards a drier and more variable climate, most prominently during the last 200 kyr, which is also reflected in the reducing DET and RR values (Fig. 4). The three episodes with Type 2 variability are about the same length (45–60 kyr) but have (according to the long-term trend) decreasing average humidity levels. The first episode is characterized by a very humid climate, while the two later episodes were rather dry. In particular, the DET values show several stepwise declines over the entire time series, which are not compensated by corresponding increases. The most striking declines are centered at approximately 515 kyr BP, 375 kyr BP, 410 kyr BP, 252 kyr BP and 80 kyr BP. The most dramatic increases in DET are centered at approximately 418 kyr BP, 345 kyr BP, 167 kyr BP and 100 kyr BP. The variability also increased, especially if a few larger fluctuations between 460-410 kyr, at ~335 kyr BP and at ~245 kyr BP are disregarded. In addition, the frequency of rapid transitions from dry to wet and back increases over time. The ODP 967 record shows similar trends on long time scales, whereas there are large differences on shorter time scales, especially in the degree of variability.

The different types of variability and the transitions between these types have important implications for our understanding of the availability of water. Different modes of variability would have transformed eastern Africa's environment considerably, including its vegetation and fauna, and would have shaped the habitat of hominins, including archaic and modern *H. sapiens*, in that part of the continent. The central question, however, is to what extent the different types of fluctuations observed in the environmental record of the Chew Bahir have actually had an impact on living conditions of hominins. Overall, long-term changes (>1 kyrs) would have

456 formed the living environment of hominins on a time-scale that responds to human evolution and corresponds

457 to a time window that is long enough to facilitate large-scale dispersal. The short-term fluctuations (<1 kyrs)

458 may have had dramatic consequences for populations including differential mortality/fertility of *H. sapiens*

459 down to the level of individuals, and thus short-term changes in behavior, including evasive movements to

460 more favorable habitats (e.g. Foerster et al., 2015).

461

462 To assess the impact of climate variability on people, it is worth using a well-studied younger analogue of

463 hydroclimatic transformation in eastern Africa. The most recent example of a wet-to-dry transition within Type

464 1 was the time-progressive termination of the African Humid Period (AHP, 15–5 kyr BP), which lasted several

465 hundred years in most areas (Shanahan et al., 2015; Trauth et al., 2018). At this time, a previously green, then

466 yellow Sahara was largely depopulated, but this happened quite slowly and due to the time-transgressive

467 termination rather in the form of people slowly following favorable living conditions (Kuper and Kröpelin, 2006;

468 Kröpelin et al., 2008; Shanahan et al., 2015). During this gradual transition, climate deterioration could have

469 fostered an important socio-economic transition, including the transition from hunter-gatherer to pastoralism

470 (Garcin et al., 2012; Foerster et al., 2015).

471

472 In contrast, the most recent example of a wet-to-dry transition within Type 2 is the onset of pronounced arid

473 conditions during the Younger Dryas chronozone (YD, ~12.8–11.6 kyr BP) that occurred within ~45 yr at Chew

474 Bahir (Trauth et al., 2018). Most importantly, millennial-scale transitions such as the YD happened everywhere

475 at the same time, unlike the orbital-controlled slow changes (Shanahan et al., 2015; Trauth et al., 2018). It is

476 implausible that such relatively rapid transitions triggered a fundamental societal transformation, similar to the

477 one during the termination of the AHP. Instead, climate shifts of this rapidity would allow response patterns

478 that are implementable within (less than) a life-time span, such as short-term migration towards proximal more

479 favorable living conditions. Examples of this are movements from hot dry low-lands into still vegetation-rich

480 high altitudes, or even the complete disappearance of entire local human populations due to scarcity of

481 resources (Foerster et al., 2015, 2016). The possible alternative response to environmental extremes and too

482 fast transformation is extinction/extirpation, because living conditions deteriorated so quickly that neither

483   physical nor cultural adaptation was possible. However, short-term and short-distance mobility depends (a) on

484   a number of socio-cultural conditions (= how flexible, how adaptable are groups, how are they organized?)

485   and (b) mode of climatic change (= pulsed, rapid, parallel with other areas).

Conclusions

487   We find two types of variability in the Chew Bahir record, (1) Type 1 probably reflecting the influence of a

488   precessional forcing in the lower latitudes at times of increased eccentricity, with the tendency towards extreme

489   events, and (2) Type 2 with significant century-millennium-scale variations with increasing frequency. Within

490   Type 2 of variability there are extremely fast transitions between dry and wet within a few decades or years

491   that would have exerted a high level of climatic stress on the biosphere including humans, in contrast to those

492   within Type 1 with transitions within several hundreds of years. As the body of archaeological evidence,

493   including fossils and diagnostic tools, continues to increase in the future, it will be exciting to compare potential

494   response patterns to our prosed Type 2 phases of high climatic stress and see whether changes in settlement

495   activities, cultural innovation, or even the emergence or disappearance of populations/occupancy can be

496   correlated with the climatic dimension of the complex framework in human-climate interactions.

Acknowledgements

References

Amante C, Eakins BW (2009) ETOPO1 1 Arc-Minute Global Relief Model: Procedures, Data Sources and Analysis. NOAA Technical Memorandum NESDIS NGDC-24.

Ambrose, S.H. (1998) Late Pleistocene human population bottlenecks, volcanic winter, and the differentiation of modern humans, Journal of Human Evolution 35, 115–118.

Bereiter, B., Eggleston, S., Schmitt, J., Nehrbass-Ahles, C., Stocker, T.F., Fischer, H., Kipfstuhl, S., Chappellaz, J. (2015) Revision of the EPICA Dome C CO_2 record from 800 to 600 kyr before present. Geophysical Research Letters. . doi: 10.1002/2014GL061957

Bonnefille, R. (2010) Cenozoic vegetation, climate changes and hominid evolution in tropical Africa. Global and Planetary Change, 72, 390-411.

Brandt, S.A. and E.A. Hildebrand (2005) Southwest Ethiopia as an Upper Pleistocene Refugium. Paper presented at the Workshop on the Middle Stone Age of Eastern Africa. Nairobi, Kenya and Addis Ababa, Ethiopia, July 2005.

Brovkin, V., Claussen, M., (2008) Comment on "Climate-Driven Ecosystem Succession in the Sahara: The Past 6000 Yr". Science, 322, 1326b-c.

Campisano CJ, Cohen AS, Arrowsmith JR, Asrat A, Behrensmeyer AK, Brown ET, Deino AL, Deocampo DM, Feibel CS, Kingston JD, Lamb HF, Lowenstein TK, Noren A, Olago DO, Owen RB, Pelletier JD, Potts R, Reed KE, Renaut RW, Russell JM, Russell JL, Schäbitz F, Stone JR, Trauth MH, Wynn JG (2017) The Hominin Sites and Paleolakes Drilling Project: high-resolution paleoclimate records from the East African Rift System and their implications for understanding the environmental context of hominin evolution. PaleoAnthropology 2017:1-43. https://doi.org/10.4207/PA.2017.ART104

Cane, M.A., Molnar, P. (2001) Closing of the Indonesian seaway as a precursor to east African aridification around 3–4 million years ago. Nature, 411, 157-162.

533   Cohen A, Campisano C, Arrowsmith R, Asrat A, Behrensmeyer AK, Deino A, Feibel C, Hill A, Johnson R,

534   Kingson J, Lamb H, Lowenstein T, Noren A, Olago D, Owen RB, Potts R, Reed K, Renaut R, Schäbitz F,

535   Tiercelin JJ, Trauth MH, Wynn J, Ivory S, Brady K, O'Grady R, Rodysill J, Githiri J, Russell J, Foerster V,

536   Dommain R, Rucina S, Deocampo D, Russell J, Billingsley A, Beck C, Dorenbeck G, Dullo L, Feary D,

537   Garello D, Gromig R, Johnson T, Junginger A, Karanja M, Kimburi E, Mbuthia A, McCartney T, McNulty E,

538   Muiruri V, Nambiro E, Negash EW, Njagi D, Wilson JN, Rabideaux N, Raub T, Sier MJ, Smith P, Urban J,

539   Warren M, Yadeta M, Yost C, Zinaye B (2016) The Hominin Sites and Paleolakes Drilling Project: Inferring

540   the Environmental Context of Human Evolution from Eastern African Rift Lake Deposits. Scientific Drilling

541   21:1-16. https://doi.org/10.5194/sd-21-1-2016.

542   Clarke, J., Brooks, N., Banning, E.B., Bar-Matthews, M., Campbell, S., Clare, L., Cremaschi, M., di Lernia, S.,

543   Drake, N., Gallinaro, M., Manning, S., Nicoll, K., Philip, G., Rosen, S., Schoop, U.D., Tafuri, M.A., Weninger,

544   B., Zerboni, A. 2016. Climatic changes and social transformations in the Near East and North Africa during

545   the 'long' 4th millennium BC: A comparative study of environmental and archaeological evidence.

546   Quaternary Science Reviews, 136, 96–121. https://doi.org/10.1016/j.quascirev.2015.10.003.

547   Davidson A (1983) The Omo River project: reconnaissance geology and geochemistry of parts of Ilubabor,

548   Kefa, Gemu Gofa and Sidamo. Ethiopian Institute of Geological Surveys Bulletin 2:1-89.

549   deMenocal, P. (1995) Plio-Pleistocene African Climate. Science 270, 53-59.

550   deMenocal P, Ortiz J, Guilderson T, Adkins J, Sarnthein M, Baker L, Yarusinsky M (2000) Abrupt onset and

551   termination of the African Humid Period: rapid climate responses to gradual insolation forcing. Quaternary

552   Science Reviews 19:347-361. https://doi.org/10.1016/S0277-3791(99)00081-5

553   deMenocal, P.B. (2004) African climate change and faunal evolution during the Pliocene-Pleistocene. Earth

554   and Planetary Science Letters 220, 3-24.

555   Ditlevsen PD, Johnsen SJ (2010) Tipping points: Early warning and wishful thinking. Geophysical Research

556   Letters 37:L19703. https://doi.org/10.1029/2010GL044486

557   Eckmann JP, Kamphorst SO, Ruelle D (1987) Recurrence Plots of Dynamical Systems. Europhysics Letters,

558   5, 973-977. https://doi.org/10.1209/0295-5075/4/9/004

559 Flohr, P., Fleitmann, D., Matthews, R., Matthews W., Black, S. 2016. Evidence of resilience to past climate
560   change in Southwest Asia: Early farming communities and the 9.2 and 8.2 ka events. Quaternary Science
561   Reviews, 136, 23–39. https://doi.org/10.1016/j.quascirev.2015.06.022.

562 Foerster V, Junginger A, Langkamp O, Gebru T, Asrat A, Umer M, Lamb H, Wennrich V, Rethemeyer J,
563   Nowaczyk N, Trauth MH, Schäbitz F (2012) Climatic change recorded in the sediments of the Chew Bahir
564   basin, southern Ethiopia, during the last 45,000 yr. Quaternary International 274:25-37.
565   https://doi.org/10.1016/j.quaint.2012.06.028

566 Foerster V, Vogelsang R, Junginger A, Asrat A, Lamb HF, Schaebitz F, Trauth MH (2015) Environmental
567   Change and Human Occupation of Southern Ethiopia and Northern Kenya during the last 20,000
568   yr. Quaternary Science Reviews 129:333-340. https://doi.org/10.1016/j.quascirev.2015.10.026

569 Foerster V, Deocampo DM, Asrat A, Günter C, Junginger A, Kraemer H, Stroncik NA, Trauth MH (2018) Towards
570   an understanding of climate proxy formation in the Chew Bahir basin, southern Ethiopian Rift. Palaeogeography,
571   Palaeoclimatology, Palaeoecology 501:111-123. https://doi.org/10.1016/j.palaeo.2018.04.009

572 Foerster et al. (submitted) 650 Thousand Years of Climate Change from Chew Bahir, S Ethiopia, and human
573   evolution, migration and innovation. Nature, submitted.

574 Fritsch, F.N., Carlson, R.E. (1980). Monotone Piecewise Cubic Interpolation. SIAM Journal on Numerical
575   Analysis, 17, 238–246.

576 Galway-Witham, J., Cole, J., Stringer, C. (2019) Aspects of human physical and behavioural evolution during
577   the last 1 million years. Journal of Quaternary Science, 34, 355–378. https://doi.org/10.1002/jqs.3137.

578 Garcin, Y., Melnick, D., Strecker, M.R., Olago, D., Tiercelin, J.-J. (2012) East African mid-Holocene wet–dry
579   transition recorded in palaeo-shorelines of Lake Turkana, northern Kenya Rift. Earth and Planetary Science
580   Letters, 331-332, 322–334.

581 Gatto, M.C., Zerboni, A. 2015. Holocene Supra-Regional Environmental Changes as Trigger for Major Socio-
582   Cultural Processes in Northeastern Africa and the Sahara. African Archaeological Review, 32, 301–333.
583   https://doi.org/10.1007/s10437-015-9191-x.

584   Grant, K.M., Rohling, E.J., Westerhold, H., Zabel, M., Heslop, D., Konijnendijk, T., Lourens, L. (2017) A 3

585   million year index for North African humidity/aridity and the implication of potential pan-African Humid

586   periods. Quaternary Science Reviews, 171, 100–118, doi: 10.1016/j.quascirev.2017.07.005.

587   Hays, J.D., Imbrie, J., Shackleton, N.J. (1976). Variations in the Earth's orbit: pacemaker of the ice ages.

588   Science, 194, 1121-1132, doi: 10.1126/science.194.4270.1121.

589   Iwanski J, Bradley E (1998) Recurrence plot analysis: To embed or not to embed? Chaos 8:861-871.

590   https://doi.org/10.1063/1.166372.

591   Junginger, A., Trauth, M.H. (2013) Hydrological constraints of paleo-Lake Suguta in the Northern Kenya Rift

592   during the African Humid Period (15 - 5 ka BP). Global and Planetary Change, 111, 174–188.

593   Kröpelin, S., Verschuren, D., Lézine, A.-M., Eggermont, H., Cocquyt, C., Francus,P., Cazet, J.-P., Fagot, M.,

594   Rumes, B., Russell, J.M., Darius, F., Conley, D.J., Schuster, M., von Suchodoletz, H., Engstrom, D.R.

595   (2008a) Climate-Driven Ecosystem Succession in the Sahara: The Past 6000 Yr. Science 320, 765-768.

596   Kröpelin, S., Verschuren, D., Lézine, A.-M. (2008b) Response to Comment by Brovkin and Claussen on

597   "Climate-Driven Ecosystem Succession in the Sahara: The Past 6000 Yr". Science, 322, 1326.

598   Kuper, R., Kröpelin, S. (2006) Climate-Controlled Holocene Occupation in the Sahara: Motor of Africa's

599   Evolution. Science, 313, 803-307.

600   Lahr, M. 2016. The shaping of human diversity: filters, boundaries and transitions. Philosophical Transactions

601   of the Royal Society B, 371: 20150241. https://10.1098/rstb.2015.0241.

602   Laskar, J., Gastineau, M., Joutel, F., Robutel, P., Levrard, B., Correia, A. (2004) A long term numerical solution

603   for the insolation quantities of Earth. Astronomy and Astrophysics, 428, 261–285.

604   Lenton TM, Held H, Kriegler E, Hall JW, Lucht W, Rahmstorf S, Schellnhuber HJ (2008) Tipping elements in

605   the Earth's climate system. Proceedings of the National Academy of Sciences 105:1786-1796.

606   https://doi.org/10.1073/pnas.0705414105

607   Marwan N, Romano MC, Thiel M, Kurths J (2007) Recurrence Plots for the Analysis of Complex Systems.

608   Physics Reports 438:237-329. https://doi.org/10.1016/j.physrep.2006.11.001

609   Marwan N (2008) A Historical Review of Recurrence Plots. European Physical Journal, Special Topics 164:3-

610   12. https://doi.org/10.1140/epjst/e2008-00829-1

611 Marwan N (2011) How to avoid potential pitfalls in recurrence plot based data analysis. Journal of Biofurcation
612   and Chaos 21:1003-1017. https://doi.org/10.1142/S0218127411029008

613 Maslin, M.A., Trauth, M.H. (2009) Plio-Pleistocene Eastern African Pulsed Climate Variability and its influence
614   on early human evolution. In: Grine, F.E., Leakey, R.E., Fleagle, J.G. (Eds.), The First Humans–Origins of
615   the Genus Homo. Springer Verlag, Vertebrate Paleobiology and Paleoanthropology Series, pp. 151-158.

616 McDougall, I., Brown, F.H., Fleagle, J.G. (2005) Stratigraphic placement and age of modern humans from
617   Kibish, Ethiopia. Nature 433, 733–736.

618 Moore JM, Davidson A (1978) Rift structure in southern Ethiopia. Tectonophysics 46:159-173.
619   https://doi.org/10.1016/0040-1951(78)90111-7.

620 Nicholson SE (2017) Climate and climatic variability of rainfall over eastern Africa. Reviews of Geophysics
621   55:590-635. https://doi.org/10.1002/2016RG000544.

622 Ossendorf et al. (2019) Middle Stone Age foragers resided in high elevations of the glaciated Bale Mountains,
623   Ethiopia. Science 365, 583–587. https://doi.org/10.1126/science.aaw8942.

624 Packard NH, Crutchfield JP, Farmer JD, Shaw RS (1980) Geometry from a time series. Physical Review
625   Letters 45:712-716. https://doi.org/10.1103/PhysRevLett.45.712

626 Potts, R. (1996) Evolution and Climate Variability. Science, 273, 922-923.

627 Potts, R. (2013) Hominin evolution in settings of strong environmental variability. Quaternary Science Reviews,
628   73, 1-13. https://doi.org/10.1016/j.quascirev.2013.04.003.

629 Scerri, E.M.L., et al. (2018) Did Our Species Evolve in Subdivided Populations across Africa, and Why Does
630   It Matter? Trends in Ecology & Evolution, 33, 592–594, 10.1016/j.tree.2018.05.005.

631 Stringer, C., Galway-Witham, J. (2017) On the origin of our species. Nature, 546, 212–214.
632   https://doi.org/10.1038/546212a.

633 Takens F (1981) Detecting strange attractors in turbulence. Lecture Notes in Mathematics 898, Springer, Berlin
634   Heidelberg New York, pp. 366-381. https://doi.org/10.1007/BFb0091924

635 Roberts et al. (submitted) Using multiple chronometers to establish a long, directly-dated lacustrine record:
636   constraining >600,000 years of environmental change at Chew Bahir, Ethiopia. QSR, submitted

637 Shanahan, T.M., McKay, N.P., Hughen, K.A., Overpeck, J.T., Otto-Bliesner, B., Heil, C.W., King, J., Scholz,
638   C.A., Peck, J. (2015) The time-transgressive termination of the African Humid Period. Nature Geoscience,
639   8, 140-144.

640 Schäbitz et al. (submitted) Two modes of humidity fluctuations in the last 200 kyr of the Chew Bahir record:
641   their meaning for migration, vertical mobility and dispersal pathways of Homo sapiens. Geology, submitted.

642 Stringer, C., Galway-Witham, J. (2017) On the origin of our species. Nature, 546, 212–213,
643   doi:10.1038/546212a.

644 Takens F (1981) Detecting strange attractors in turbulence. Lecture Notes in Mathematics 898, Springer, Berlin
645   Heidelberg New York, pp. 366-381. https://doi.org/10.1007/BFb0091924

646 Tierney JE, deMenocal PB (2013) Abrupt shifts in Horn of Africa hydroclimate since the last glacial maximum.
647   Science 342:843-846. https://doi.org/10.1126/science.1240411

648 Trauth, M.H., Maslin, M.A., Deino, A., Strecker, M.R. (2005) Late Cenozoic Moisture History of Eastern Africa.
649   Science, 309, 2051-2053.

650 Trauth, M.H., Larrasoaña, J.C., Mudelsee, M. (2009) Trends, rhythms and events in Plio-Pleistocene African
651   climate. Quaternary Science Reviews, 28, 399-411.

652 Trauth, M.H., Maslin, M.A., Deino, A., Junginger, A., Lesoloyia, M., Odada, E., Olago, D.O., Olaka, L., Strecker,
653   M.R., Tiedemann, R. (2010) Human Evolution in a Variable Environment: The Amplifier Lakes of East
654   Africa. Quaternary Science Reviews, 29. 2981-2988.

655 Trauth MH, Bergner AGN, Foerster V, Junginger A, Maslin MA, Schaebitz F (2015) Episodes of environmental
656   stability and instability in late Cenozoic lake records of Eastern Africa. Journal of Human Evolution 87:21-
657   31. https://doi.org/10.1016/j.jhevol.2015.03.011

658 Trauth MH, Foerster V, Junginger A, Asrat A, Lamb HF, Schaebitz F (2018) Abrupt or gradual? Change point
659   analysis of the late Pleistocene-Holocene climate record from Chew Bahir, southern Ethiopia. Quaternary
660   Research 90:321-330. https://doi.org/10.1017/qua.2018.30

661 Trauth, M.H., Asrat, A., Duesing, W., Foerster, V., Kraemer, K.H., Marwan, N., Maslin, M.A., Schaebitz, F.
662   (2019) Classifying past climate change in the Chew Bahir basin, southern Ethiopia, using recurrence
663   quantification analysis. Climate Dynamics, available online, https://doi.org/10.1007/s00382-019-04641-3.

664   Viste, E., Sorteberg, A. (2013) The effect of moisture transport variability on Ethiopian summer precipitation.

665   International Journal of Climatology, 33, 3107-312. https://doi.org/10.1002/joc.3566.

666   Vogelsang, R., Bubenzer, O., Kehl, M., Meyer, S., Richter, J., Zinaya, B. (2018) When Hominins Conquered

667   Highlands—an Acheulean Site at 3000 m a.s.l. on Mount Dendi/Ethiopia. Journal of Paleolithic Archaeology

668   1, 302–313. https://doi.org/10.1007/s41982-018-0015-9.

669   Vrba, E.S. (1985) Environment and evolution: Alternative causes of the temporal distribution of evolutionary

670   events. South African Journal of Sciences 81, 229–236.

671   Vrba, E.S., (1993) The pulse that produced us: two major global coolings may have prodded antelopes and

672   humans to evolve : How did humans get that way? Natural History 102 (5), 47-51.

673   Webber CL, Zbilut JP (2005) Recurrence Quantification Analysis of Nonlinear Dynamical Systems, in: from:

674   Riley, M.A, Van Orden, G.C, Tutorials in contemporary nonlinear methods for the behavioral sciences,

675   https://doi.org/10.1007/978-3-319-07155-8

676   Wessel P, Smith WHF (1996) A Global Self-consistent, Hierarchical, High-resolution Shoreline Database.

677   Journal of Geophysical Research 101 B4: 8741-8743.

678   Zbilut JP, Webber Jr CL (1992) Embeddings and delays as derived from quantification of recurrence plots.

679   Physics Letters A 171:199-203. https://doi.org/10.1016/0375-9601(92)90426-M
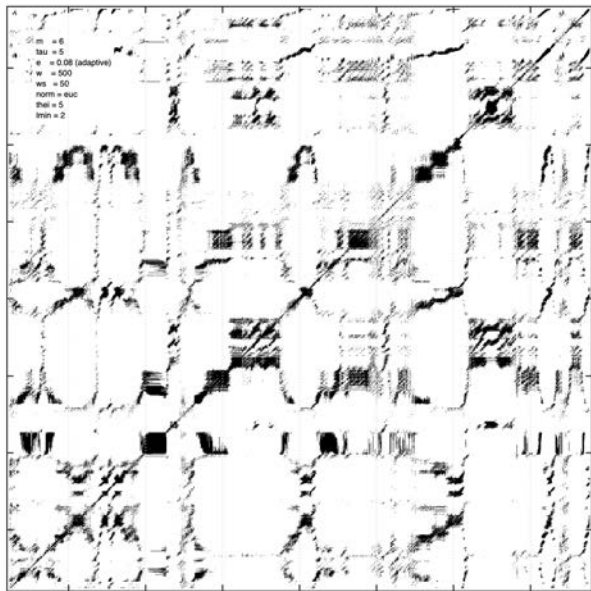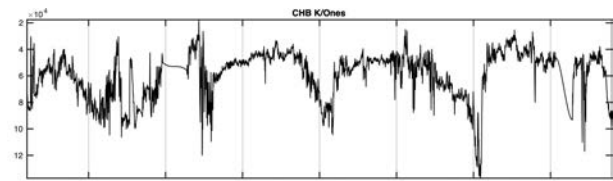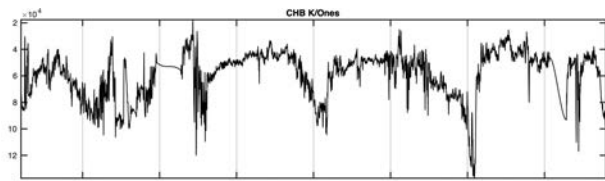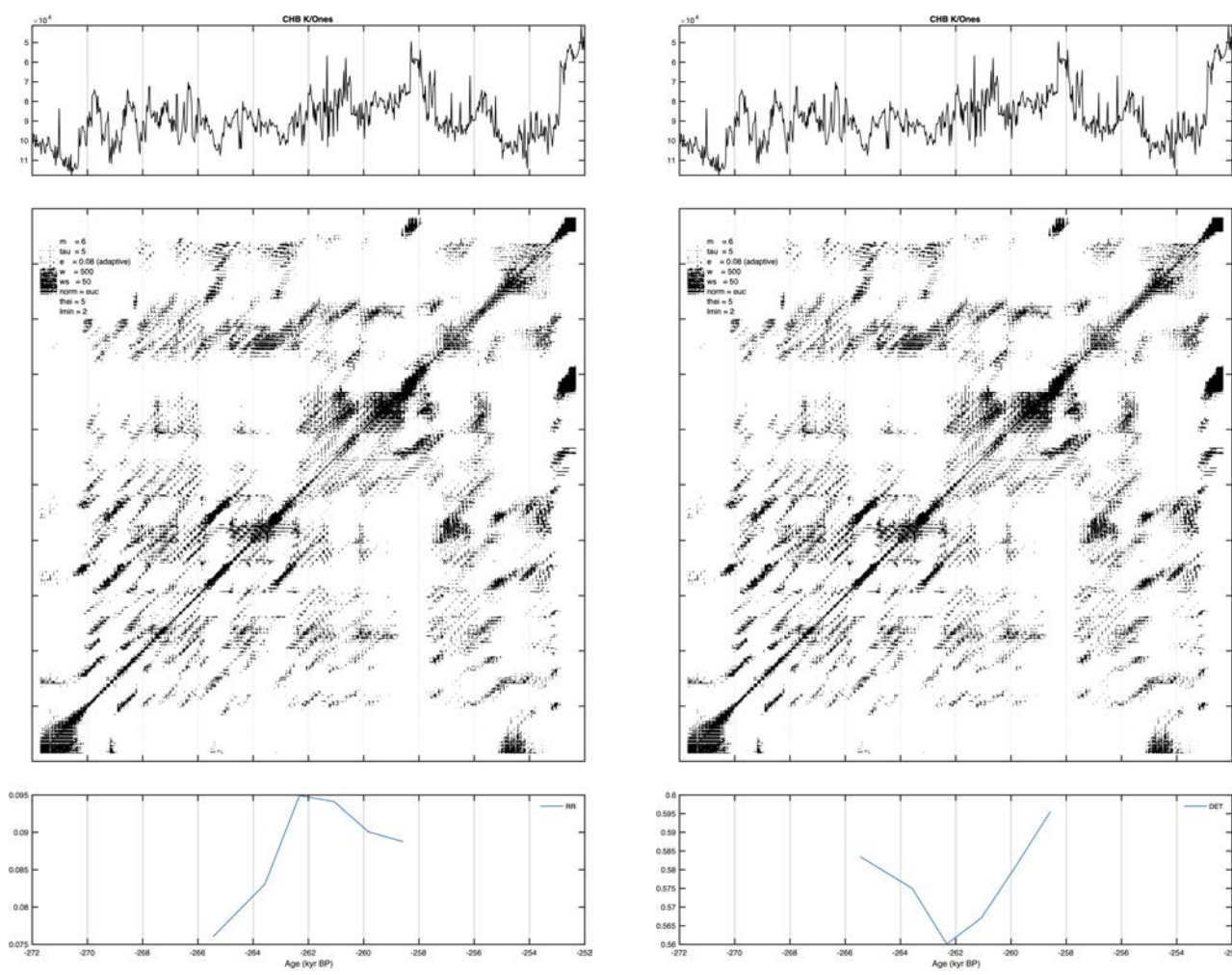
Supplementary Material

681
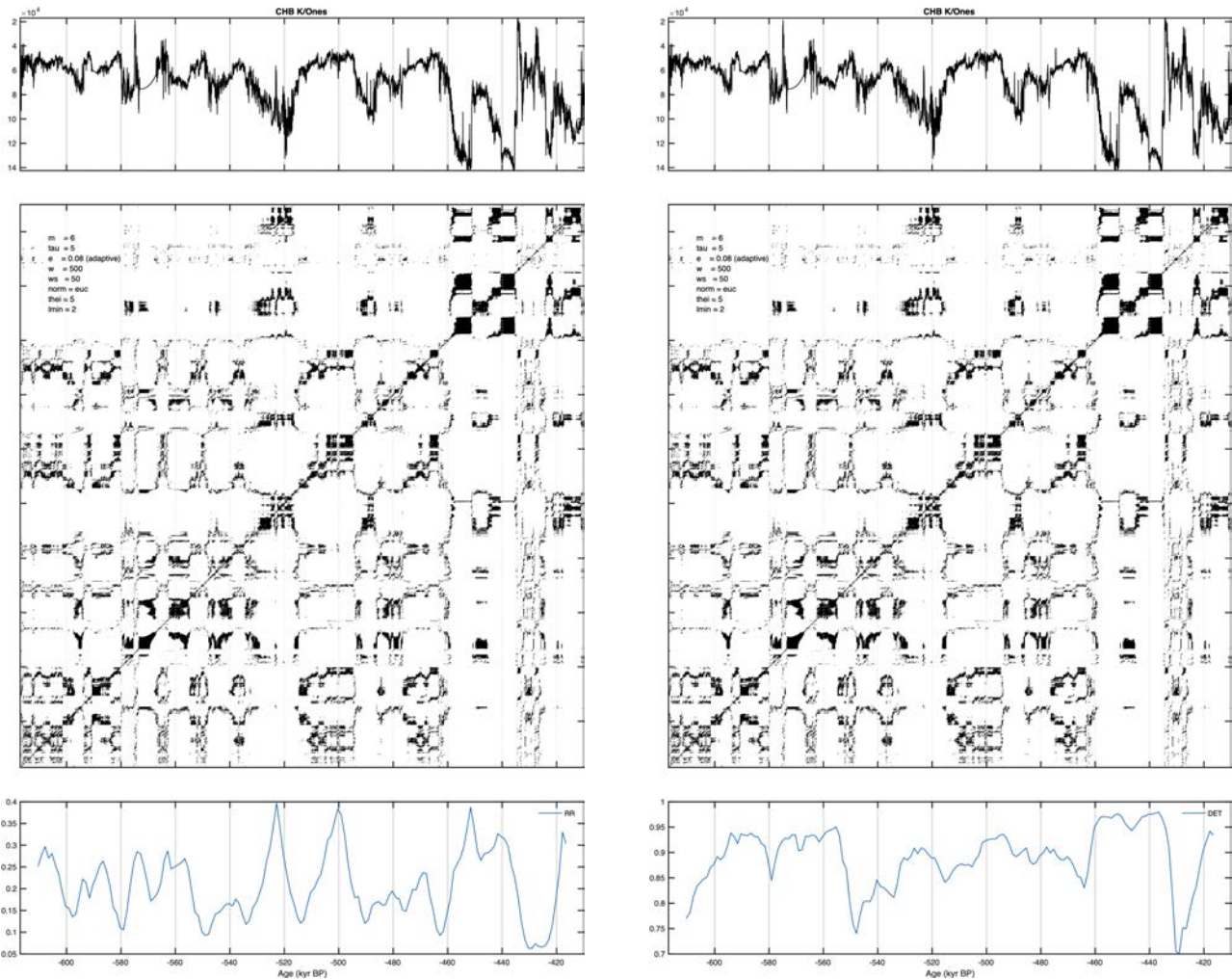
682
683

684 **Supplementary Figure 1** Recurrence plot (RP) and recurrence quantification analysis (RQA) measures of the
685 high resolution (0.015 kyr) potassium (K) concentrations of the sediment in Chew Bahir in southern Ethiopia
686 between 620 and 410 kyr BP: the time series according to age model (3) (upper panel), the recurrence plot
687 (middle panel) and the RQA measures **(a)** RR and **(b)** DET of moving windows (lower panel). Embedding
688 parameters *m*=embedding dimension, *tau*=time delay, *e*=threshold, *w*=window size, *ws*=window moving steps,
689 *norm*=vector norm, *thei*=size of Theiler window, *lmin*=minimum line length, RQA measures *RR*=recurrence
690 rate and *DET*=determinism. See the methods section for a detailed description of the embedding parameters
691 and RQA measures.
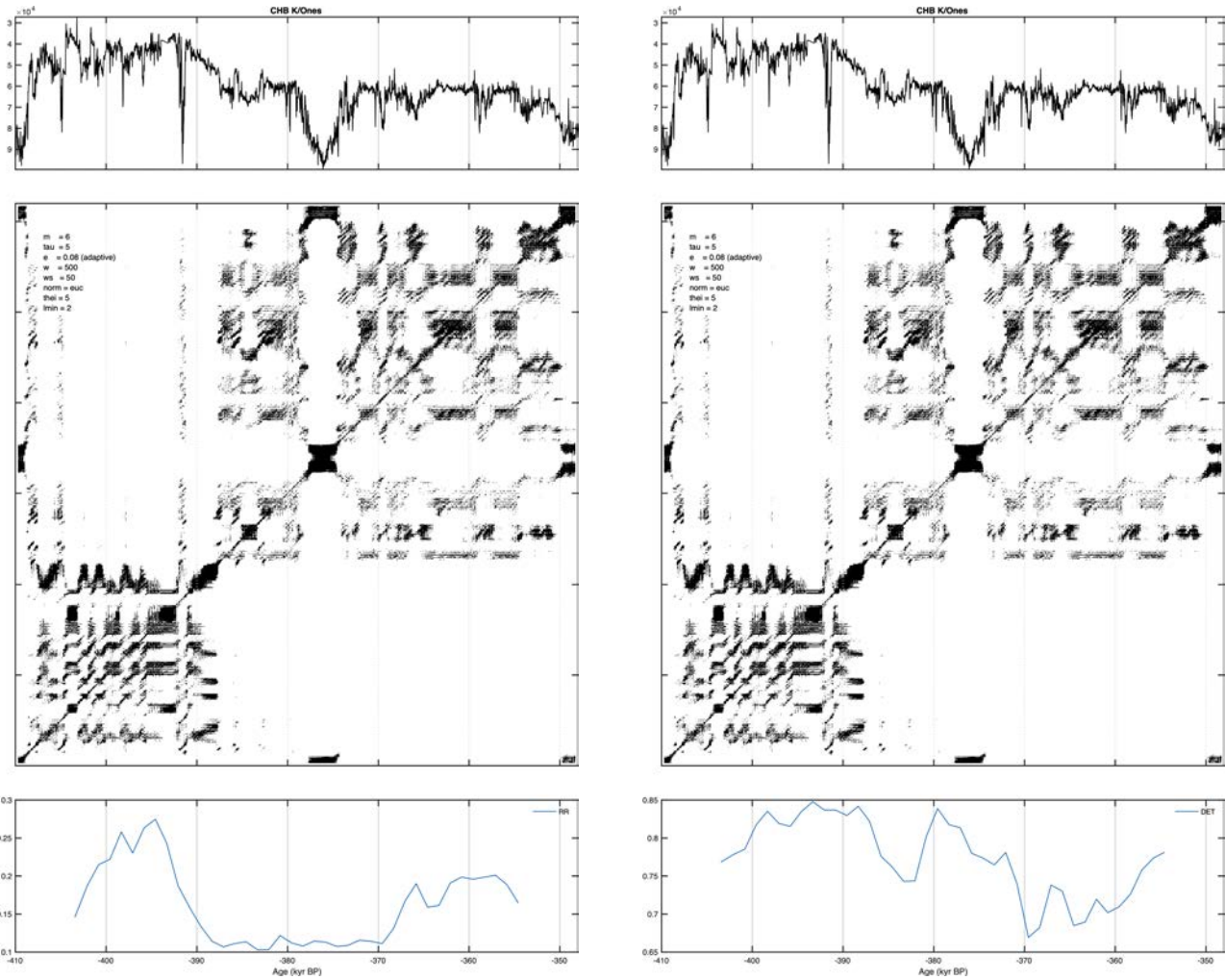
692
693
694 **Supplementary Figure 2** Recurrence plot (RP) and recurrence quantification analysis (RQA) measures of the
695 high resolution (0.015 kyr) potassium (K) concentrations of the sediment in Chew Bahir in southern Ethiopia
696 between 410 and 348 kyr BP: the time series according to age model (3) (upper panel), the recurrence plot
697 (middle panel) and the RQA measures **(a)** RR and **(b)** DET of moving windows (lower panel). For
698 abbreviations, see caption of Supplementary Figure 1. See the methods section for a detailed description of
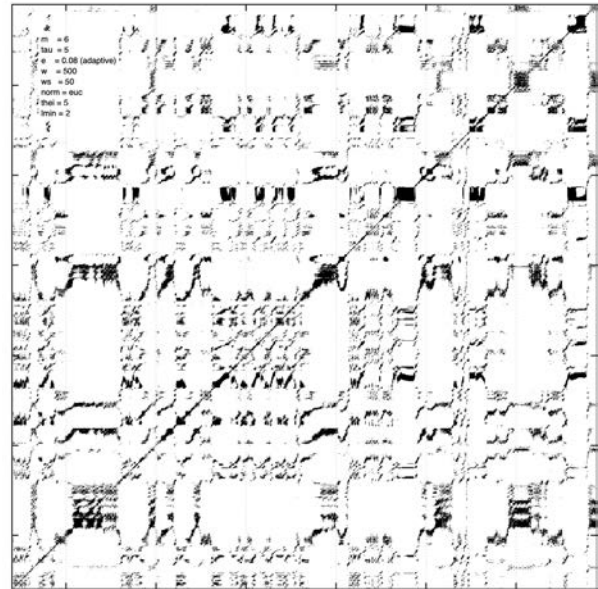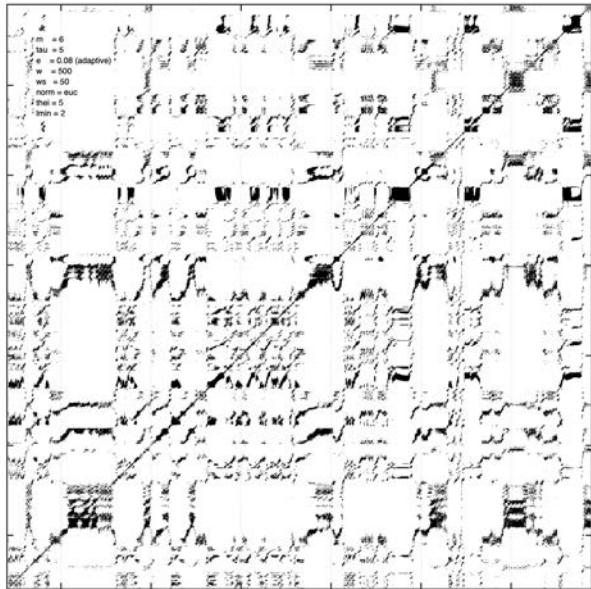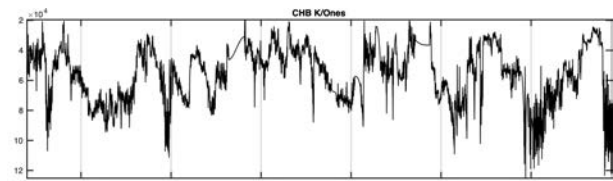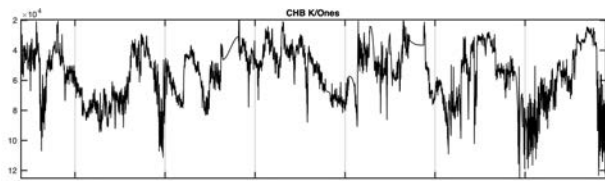699 the embedding parameters and RQA measures.
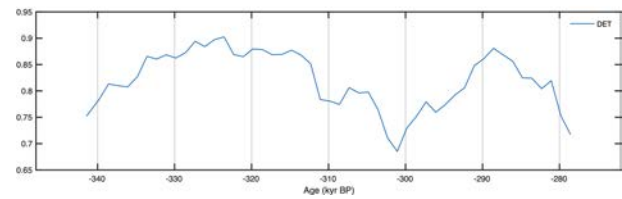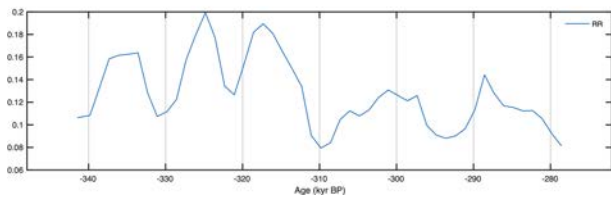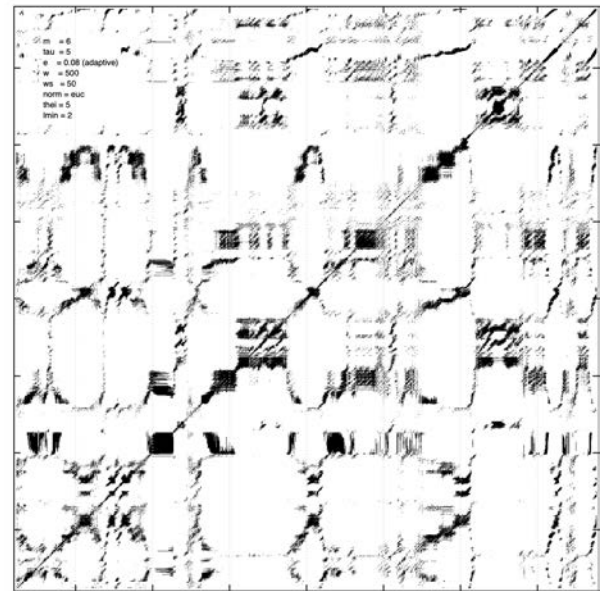
700
701

702 **Supplementary Figure 3** Recurrence plot (RP) and recurrence quantification analysis (RQA) measures of the

703 high resolution (0.015 kyr) potassium (K) concentrations of the sediment in Chew Bahir in southern Ethiopia

704 between 348 and 272 kyr BP: the time series according to age model (3) (upper panel), the recurrence plot

705 (middle panel) and the RQA measures **(a)** RR and **(b)** DET of moving windows (lower panel). For

706 abbreviations, see caption of Supplementary Figure 1. See the methods section for a detailed description of

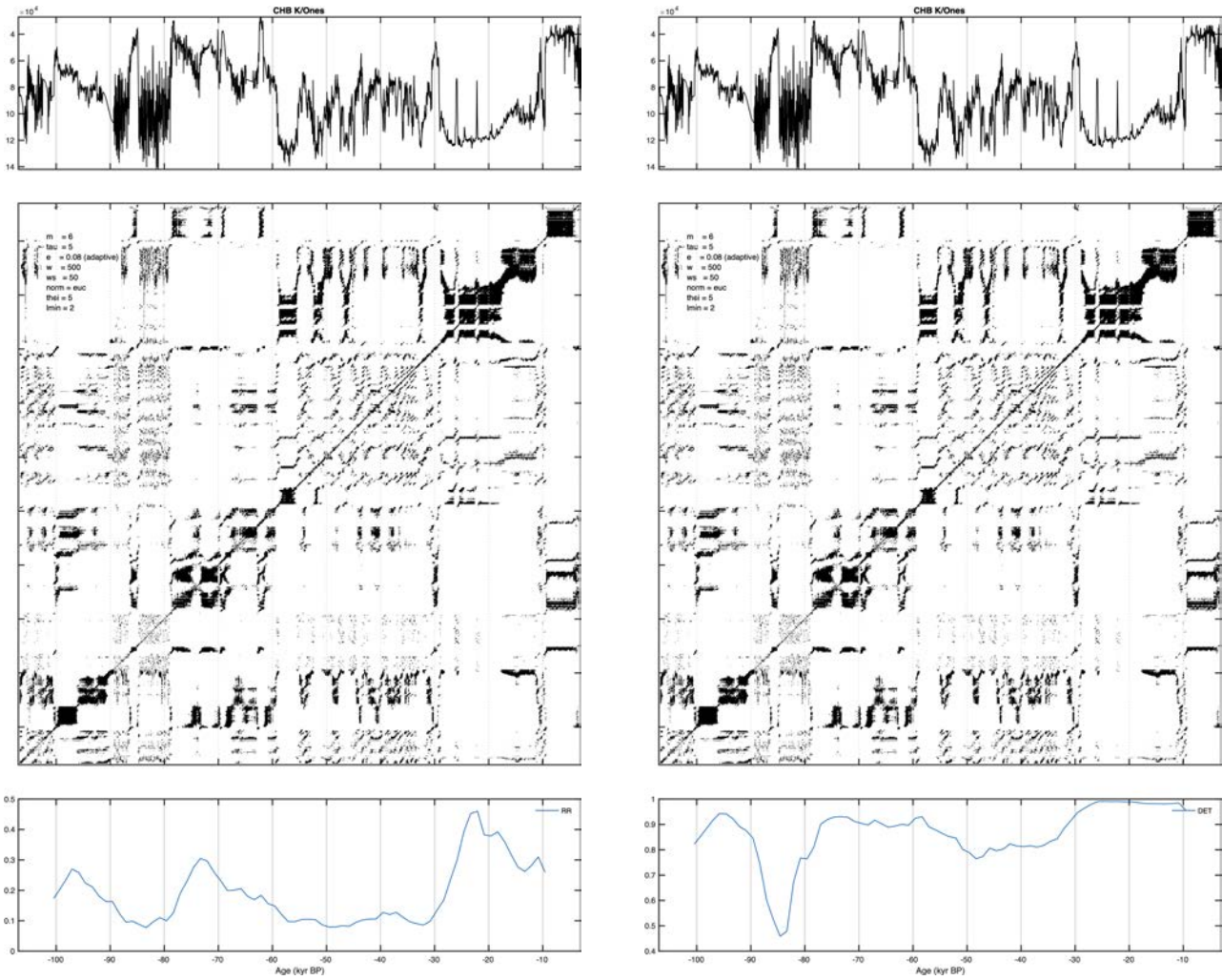707 the embedding parameters and RQA measures.

708

709

710 **Supplementary Figure 4** Recurrence plot (RP) and recurrence quantification analysis (RQA) measures of the

711 high resolution (0.015 kyr) potassium (K) concentrations of the sediment in Chew Bahir in southern Ethiopia

712 between 272 and 252 kyr BP: the time series according to age model (3) (upper panel), the recurrence plot

713 (middle panel) and the RQA measures **(a)** RR and **(b)** DET of moving windows (lower panel). For

714 abbreviations, see caption of Supplementary Figure 1. See the methods section for a detailed description of

715 the embedding parameters and RQA measures.
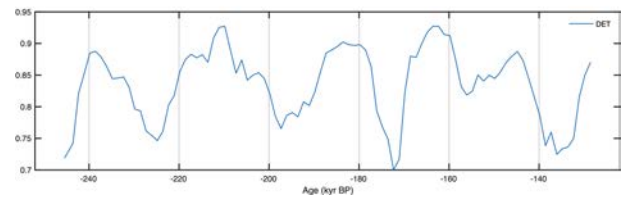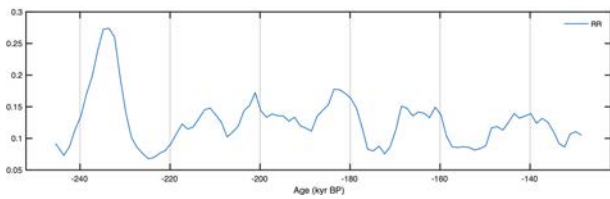
716
717
718 **Supplementary Figure 5** Recurrence plot (RP) and recurrence quantification analysis (RQA) measures of the
719 high resolution (0.015 kyr) potassium (K) concentrations of the sediment in Chew Bahir in southern Ethiopia
720 between 252 and 122 kyr BP: the time series according to age model (3) (upper panel), the recurrence plot
721 (middle panel) and the RQA measures **(a)** RR and **(b)** DET of moving windows (lower panel). For
722 abbreviations, see caption of Supplementary Figure 1. See the methods section for a detailed description of
723 the embedding parameters and RQA measures.

724
725

726 **Supplementary Figure 6** Recurrence plot (RP) and recurrence quantification analysis (RQA) measures of the
727 high resolution (0.015 kyr) potassium (K) concentrations of the sediment in Chew Bahir in southern Ethiopia
728 between 107 and 3 kyr BP: the time series according to age model (3) (upper panel), the recurrence plot
729 (middle panel) and the RQA measures **(a)** RR and **(b)** DET of moving windows (lower panel). For
730 abbreviations, see caption of Supplementary Figure 1. See the methods section for a detailed description of
731 the embedding parameters and RQA measures.